Real-time kinematic positioning algorithm with GNSS and high-frequency accelerometer observations for broadband signals

Rui Tu[1,2,3,4] ⓘ**, Jinhai Liu**[1,2]**, Rui Zhang**[1,3]**, Lihong Fan**[1,3]**, Pengfei Zhang**[1,2] ⓘ
and Junqiang Han[1,3]

[1] National Time Service Center, Chinese Academy of Sciences, Shu Yuan Road, Xi'an 710600,
People's Republic of China
[2] University of Chinese Academy of Sciences, Yu Quan Road, Beijing 100049,
People's Republic of China
[3] Key Laboratory of Precision Navigation Positioning and Timing Technology,
Chinese Academy of Sciences, Xi'an 710600, People's Republic of China

E-mail: turui-2004@126.com

Abstract

Real-time kinematic (RTK) positioning technology is widely used for deformation monitoring, but the signals of high-frequency band such as velocity and acceleration are easily polluted due to the bad signal to noise ratio. In order to obtain high-precision and broadband signals for deformation monitoring, we propose an enhanced RTK positioning algorithm by adding high-frequency accelerometer observations and estimate the bias of the acceleration as an unknown parameter in real-time. In addition, a dataset was constructed based on an experiment and used for the validation of our approach. The experiment is operated on a platform and includes a dynamic Global Navigation Satellite System (GNSS) antenna, a low-cost micro-electro-mechanical system (MEMS)-type accelerometer and a slide rail. We conducted eight simulations by sliding the collocated GNSS antenna and MEMS from one point to the other point by manual operation to record 2D movements in horizontal components. A vernier caliper was also set up to estimate the reference displacement for comparison, the maximum sliding distance of the platform is restricted to about 0.5 m. Our validation analyses demonstrate that the enhanced RTK positioning algorithm can provide high-precision displacement, velocity, and acceleration signals in real-time. The average accuracies are 5.0 mm, 0.6 mm s^{-1} and 1.0 mm s^{-2} respectively. Furthermore, the high-resolution acceleration signal from the MEMS is helpful to improve the RTK ambiguity resolution because the R-ratio (the ratio of the second minimum to the minimum quadratic form of residuals) values achieved by the new approach are much larger than the standard RTK approach.

Keywords: real-time kinematic positioning, broadband signals, GNSS, ambiguity resolution, baseline error, deformation monitoring

(Some figures may appear in colour only in the online journal)

---

[4] Author to whom any correspondence should be addressed.

1. Introduction

The real-time kinematic positioning (RTK) technology that uses double-difference (DD) observations to eliminate or reduce common errors such as satellite orbit, clock, and atmosphere errors for the short baselines (Wellenhof *et al* 2001), and recovers the integer feature of the DD carrier phase ambiguity, has a positioning accuracy in the range of millimeters to centimeters after the fast ambiguity resolution (Rizos 2007). Takasu *et al* provided an open source program package named RTKLIB, which can reach to the accuracy of centimeters whether for low-cost receivers or long baseline RTK users (Takasu *et al* 2009, 2010). The RTK performance with raw observations for BeiDou Navigation Satellite System (BDS) has been tested by Tu *et al*, and the accuracy is 1-2 centimeters (Tu *et al* 2017a, 2019). Owing to its characteristics of high precision, fast initialization, and ease of real-time application, it has been widely used for local area deformation monitoring (Tu *et al* 2017b), including monitoring of landslides, bridges, dams and buildings (Uhlemann *et al* 2006).

In particular, for the deformation monitoring application, both low-frequency and high-frequency signals are considered important. However, RTK can only provide low-frequency displacement signals with high precision, it cannot provide high-frequency signals, such as velocity and acceleration precisely because the Global Navigation Satellite System (GNSS) also records noise (Genrich *et al* 2006). Elosegui *et al* used the modified sidereal filtering to deal with the noises (Elosegui *et al* 2006). Larson *et al* used the aspect repeat time adjustment method to reduce the multipath noises and improve the precision of high-rate GNSS (Larson *et al* 2007).

Nevertheless, a digital accelerometer can measure strong ground motion with a considerably higher resolution than the GNSS, especially in the case of high-frequency acceleration; therefore, it is also widely used for deformation monitoring (Freybourger *et al* 1997, Wilson *et al* 2002). Wang *et al* used the digital strong-motion records to recover the static displacement (Wang *et al* 2011) and Tu *et al* used it for integration with GNSS observations to retrieve broadband ground-motion signals (Tu *et al* 2013). Thus, in this study, we present a method to include high-frequency accelerometer observations into the RTK estimation model, which might, in turn, resolve the problems of high-frequency signals pollution.

Even with its advantages, the accelerometer observations might be biased owing to the so-called baseline errors that are believed to be caused by ground vibration induced tilting of instruments (Trifunac *et al* 1971, Graizer *et al* 1979, 2006). Furthermore, these baseline errors will be magnified while integrated into velocity and/or displacement (Wang *et al* 2011, Boore *et al* 2011, Wang *et al* 2013). To mitigate these problems, typically, there are two methods for baseline error correction. The first method is empirical correction, the baseline shift is usually treated as a constant according to the time window. The details can be found in lots of literature. For example, Iwan *et al* (1985) introduced an average transient baseline offset by the empirical criterion (Zhu *et al* 2003, Zhu 2003, Wu and Wu 2007) developed Iwan's approach with different empirically based criterions (Zhu *et al* 2003, Wu

et al 2007, Chao *et al* 2009, Wang *et al* 2011) proposed an automatic scheme for baseline correction of strong-motion records (Larson *et al* 2007, Chao *et al* 2009, Melgar *et al* 2013) developed a robust and reliable automated baseline corrections for strong motion seismology. The main difference between them is how to determine the time windows (Melgar *et al* 2013), and the empirical baseline correction approach can only be applied at the post-solution stage; however, this method has low precision. The second method involves the use of other observation results like high-precision GNSS data as references to estimate the baseline errors. Bock *et al* (2011) absorbed it as dynamic noise (Bock *et al* 2011), Tu *et al* estimated it by a random walk process (Tu *et al* 2014a, 2016a, 2016b), while Geng *et al* (2013a) estimated it by a white noise and also studied how to recover coseismic point ground tilts from the collocated high-rate GPS and accelerometers (Geng *et al* 2013a, 2013b), Benedetti *et al* (2017) also used the mixed GNSS and MEMS by a Kalman filter to estimate at the same time the accelerometer bias along with the other parameters like position and velocity (Benedetti *et al* 2017). Aside from its suitability for real-time operation application, the second approach has a considerably higher precision than the empirical correction method.

Using accelerometer measurements to enhance precise point positioning (PPP) solution has been studied, but to enhance RTK solution has never been presented before (Li *et al* 2013). Considering the information mentioned above, in this study, we propose an enhanced real-time kinematic positioning (E-RTK) algorithm by the integration of GNSS and accelerometer observation to real-time get high-precision and broadband displacement, velocity and acceleration information. In our proposed approach, the high-frequency acceleration observations from the accelerometer are included in the E-RTK model; in addition, the baseline errors are estimated as unknown parameters in real-time. Our validation analyses show that the E-RTK model can provide high-precision and broadband signals (displacement, velocity, and acceleration) in real-time; in addition, high-resolution acceleration can be used to constrain the RTK solution for better ambiguity resolution.

First, the E-RTK approach is introduced. Then, the experimental datasets used for validation of our method and subsequent analysis are discussed. Finally, the conclusions and remarks are provided at the end.

2. Methodology

In this study, the DD RTK model is used for our proposed integrated approach along with the high-frequency accelerometer records; in addition, the baseline error of the accelerometer is estimated as a random walk process (Tu *et al* 2016a). In the following subsections, we introduce the observation equation, state equation, and parameter estimation strategy in that order.

2.1. Observation equation

The linearized DD pseudorange and carrier phase observation equations for the GNSS dual frequency observations at epoch k are expressed as follows:

$$P_{\text{br}}^{ij}(k) = e_{\text{r}}^{ij}(k) \cdot s_{\text{r}}(k) + I_{\text{br}}^{ij}(k) + T_{\text{br}}^{ij}(k) \\ + \rho_{\text{br}}^{ij}(k) + \varepsilon_{\text{P}}(k), \quad \varepsilon_{\text{P}} \sim N(0, \sigma_{\text{P}}^2) \tag{1}$$

$$\lambda(k) \cdot \phi_{\text{br}}^{ij}(k) = e_{\text{r}}^{ij}(k) \cdot s_{\text{r}}(k) - I_{\text{br}}^{ij}(k) + T_{\text{br}}^{ij}(k) \\ + \rho_{\text{br}}^{ij}(k) - \lambda \cdot \text{Amb}_{\text{br}}^{ij}(k) + \varepsilon_{\phi}(k), \quad \varepsilon_{\phi} \sim N(0, \sigma_{\phi}^2), \tag{2}$$

where P and Φ are the pseudorange and carrier phase observables, respectively; the subscripts b and r represent the base and user receivers, respectively, while the superscripts i and j represent the satellite number. Further, $(\cdot)_{\text{br}}^i$ and $(\cdot)_{\text{br}}^j$ express the single-difference (SD) between stations, whereas $(\cdot)_{\text{br}}^{ij}$ is the DD between the stations and satellites. The symbol e is the unit vectors along the line of sight from the receiver to satellite. The coordinate baseline components s are to be solved for, Amb is the integer ambiguity of the carrier phase, and I and T are the ionospheric delay and tropospheric delay, respectively. ε is the measurement noise with the standard deviation σ, while ρ is the geometric distance from the satellite to receiver.

As the acceleration records contain baseline shift, the acceleration equations are expressed as follows:

$$L_{\text{a}}(k) = a_k + u_k + \varepsilon_{L_{\text{a}}}(k), \quad \varepsilon_{L_{\text{a}}} \sim N(0, \sigma_{L_{\text{a}}}^2) \tag{3}$$

where L_{a} is the raw acceleration record, a denotes acceleration of the station, u denotes the baseline error of acceleration, $\varepsilon_{L_{\text{a}}}$ is the measurement noise of L_{a} and its standard deviation is $\sigma_{L_{\text{a}}}$. Usually, the baseline error of acceleration is corrected by the empirical approach (Iwan *et al* 1985), we estimated it as an unknown parameter in this study.

2.2. Stochastic model

The stochastic model is determined by the observation noise and satellite elevations (Guo *et al* 2016), which can be expressed as follows:

$$D = \begin{matrix} \sigma_{\text{P}}^2/\sin^2(E) \\ \sigma_{\phi}^2/\sin^2(E) \\ \sigma_{L_{\text{a}}}^2. \end{matrix} \tag{4}$$

σ_{P}, σ_{ϕ} and $\sigma_{L_{\text{a}}}$ are the standard deviations of the measurement noise for the pseudorange, carrier phase and acceleration observations respectively, and E is the satellite elevation in unit of rad.

2.3. State equation

Because RTK is typically used for local area monitoring involving just several kilometers, the DD ionosphere and troposphere residuals can be neglected in this condition. The carrier phase ambiguity is a constant in a continuous period so it can be ignored in the state equation. Thus, here, we only discuss the state equations for the displacement, velocity, acceleration, and baseline error.

The state equation of the standard RTK (S-RTK) can be represented using the two-order Gaussian–Markov process as follows:

$$\begin{bmatrix} s \\ v \\ a \end{bmatrix}_k = \begin{bmatrix} 1 & \tau & {}^1\!/_2\tau^2 \\ 0 & 1 & \tau \\ 0 & 0 & 1 \end{bmatrix} \cdot \begin{bmatrix} s \\ v \\ a \end{bmatrix}_{k-1} + \alpha_k, \quad \alpha_k \sim N(0, Q^s) \tag{5}$$

$$[Q^s] = \begin{bmatrix} {}^1\!/_{20}\tau^5 q_{\text{a}} & {}^1\!/_8\tau^4 q_{\text{a}} & {}^1\!/_6\tau^3 q_{\text{a}} \\ {}^1\!/_8\tau^4 q_{\text{a}} & {}^1\!/_3\tau^3 q_{\text{a}} & {}^1\!/_2\tau^2 q_{\text{a}} \\ {}^1\!/_6\tau^3 q_{\text{a}} & {}^1\!/_2\tau^2 q_{\text{a}} & \tau q_{\text{a}} \end{bmatrix} \tag{6}$$

where τ is the sample rate of the GNSS, α is the dynamic noise, and v denote the velocity of the station. Q^S represents the dynamic state noise, while q_{a} is the variance of acceleration.

With the addition of the acceleration measurements, the new state equation for our enhanced RTK algorithm can be represented in a new form.
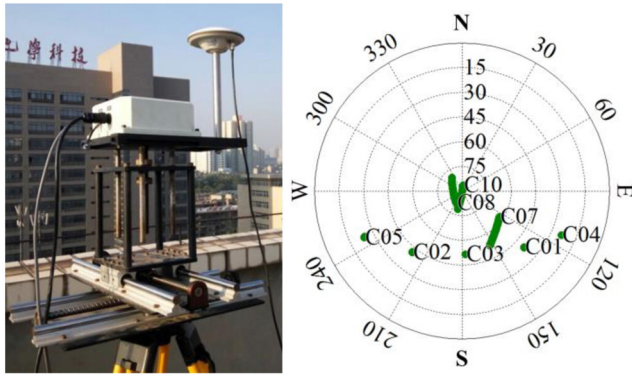
$$\begin{bmatrix} s \\ v \\ a \\ u \end{bmatrix}_k = \begin{bmatrix} 1 & \tau & {}^1\!/_2\tau^2 & 0 \\ 0 & 1 & \tau & 0 \\ 0 & 0 & 1 & 0 \\ 0 & 0 & 0 & 1 \end{bmatrix} \cdot \begin{bmatrix} s \\ v \\ a \\ u \end{bmatrix}_{k-1} + \beta_k, \quad \beta_k \sim N(0, Q^{\text{E}}) \tag{7}$$

$$[Q^{\text{E}}] = \begin{bmatrix} {}^1\!/_{20}\tau^5 q_{\text{a}} & {}^1\!/_8\tau^4 q_{\text{a}} & {}^1\!/_6\tau^3 q_{\text{a}} & 0 \\ {}^1\!/_8\tau^4 q_{\text{a}} & {}^1\!/_3\tau^3 q_{\text{a}} & {}^1\!/_2\tau^2 q_{\text{a}} & 0 \\ {}^1\!/_6\tau^3 q_{\text{a}} & {}^1\!/_2\tau^2 q_{\text{a}} & \tau q_a & 0 \\ 0 & 0 & 0 & \tau q_{\text{u}} \end{bmatrix} \tag{8}$$

where β is the dynamic noise, Q^{E} represents the dynamic state noise, and q_{u} is the variance of the baseline error.

2.4. Parameter estimation strategy

Parameter estimation is performed based on the observation equations (1)–(3), stochastic model [4] and state equations (7) and (8), using a Kalman filter (Yang *et al* 2006), the estimation details can be referenced to the former studies (Bock *et al* 2011, Tu *et al* 2014b). The solution parameters include the receiver's displacement, velocity, acceleration, baseline error, and DD carrier phase ambiguities. The standard deviations for carrier phase, pseudorange and acceleration observations are set as 0.002 m, 0.2 m and 0.01m according to the empirical signal to noise ratio, respectively. In addition, the dynamic noises q_{v}, q_{a}, and q_{u} in this study are set as 0.06 m s^{-1}, 0.006 m s^{-2}, 0.001 m s^{-2} according to the motion state, respectively. For the data solution, the displacement and velocity are estimated at each epoch based on the dynamic noise, while the baseline errors are treated as a random walk process; the carrier phase ambiguity is estimated as a constant in a continuous period; nevertheless, it is reinitialized when a cycle slip occurs. It should be noted that the GNSS sampling frequencies (1 Hz) are traditionally lower than accelerometer's sampling frequencies (100 Hz); therefore, the filter needs to be adapted to this multi-rate environment (Smyth *et al* 2006) by performing the prediction stage at every time step and

Figure 1. Experimental platform (left side) and satellite geometry (right side). (Left) Adapted with permission from Tu *et al* (2017b). © The Authors 2017. Published by Oxford.
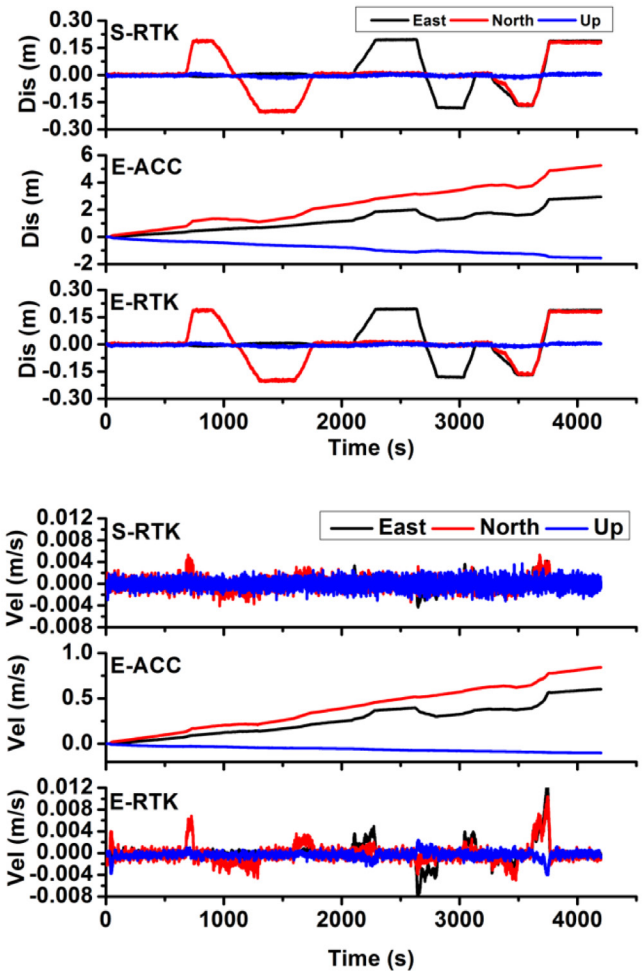
applying the filter update stage only when a GNSS sample becomes available.

Using the filter system, high-precision displacement, velocity, acceleration and baseline errors can be directly obtained in real-time.

3. Results and validations

In order to validate the performance of E-RTK algorithm, a dataset was constructed based on an experiment. The left image in figure 1 shows the platform that we used in the experiment, which was conducted in August 2016 at Xi'An, China (Tu *et al* 2017b). The platform, which can slide along a table, includes a dynamic GNSS antenna (Receiver type: UR380, Antenna: HX-GG486A) and low-cost micro-electro-mechanical system (MEMS)-type accelerometer (Type: EWM 1580) (Fleming *et al* 2009), and a slide rail. The distance between the reference station and experimental platform is about 10 m. As previously mentioned, the sampling rates for the GNSS and accelerometer are 1 Hz and 100 Hz, respectively. It should be noted that we only used the BDS data in this study to test the performance of BDS, and the multi-GNSS systems will get a better results as the better satellite geometry (Tu *et al* 2017b). The maximum sliding distance of the platform is restricted to about 0.5 m and the slide capability in term of frequency is about 1–5 Hz, the time span of the experiment is about one hour. Furthermore, the right subfigure in figure 1 shows the geometric satellite distribution during the experiment; in particular, observations from eight BDS satellites (C01, C02, C03, C04, C05, C07, C08, C10) were used. The average geometric dilution of precision (GDOP) value is 2.8.

We conducted eight simulations (namely, T1, T2, T3, T4, T5, T6, T7, and T8) by moving the platform from one point to another point along the rail. In the experiment, the platform is installed by manual operation, so it is not really in the horizontal state. In addition, while moving the instrument, the platform will cause a small waggle. These small tiltings will cause the baseline error. The reference displacements are measured using a vernier caliper that was fixed on the table; the precision of the caliper was better than 2 mm. For each experiment, we held the rig static at the starting point for
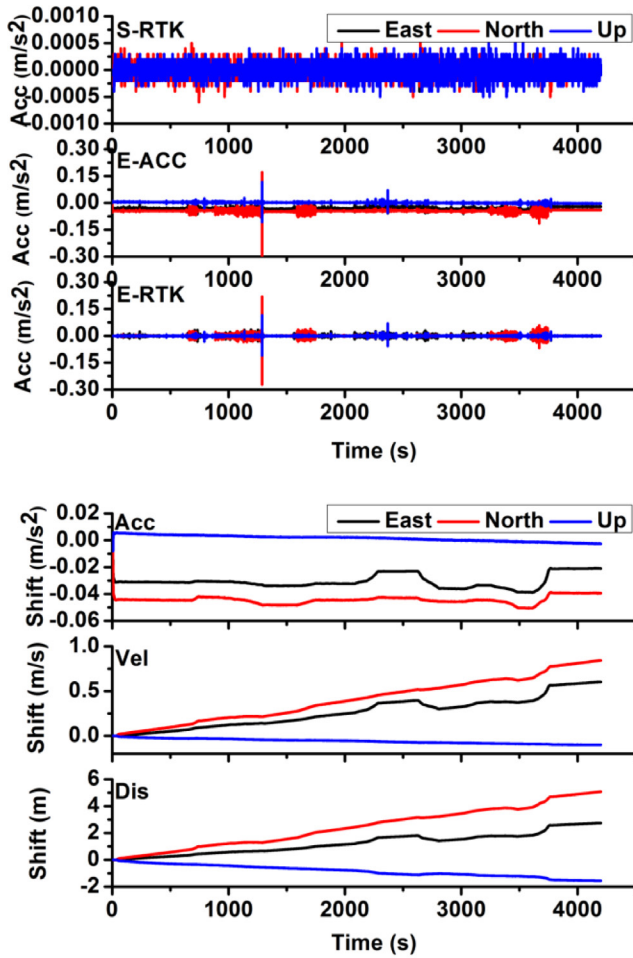

Figure 2. Comparison of displacement (top) and velocity (bottom) time series obtained using different approaches.

several minutes; then, we slid the combined instruments from the starting point to end point in about one or two minutes, after this, the rig was kept stationary again at the end point for several minutes before starting the next experiment. In summary, we conducted eight experimental simulations in the horizontal component; in particular, three times in the south–north direction, three times in the east–west direction, and two times in the south–west to north–east direction.

For the combined data solution, we need to align the coordinate reference frames and time reference frames. Firstly, transform the accelerometer's east, north and up (ENU) coordinates to the platform's local ENU coordinates, secondly, the local coordinates are converted to GNSS conventional terrestrial system coordinates (Xu *et al* 2013, Tu *et al* 2016b, Benedetti *et al* 2017). There is also a small GNSS device inside the accelerometer, which is used for the clock synchronization between accelerometer and GNSS, thus the two time systems are aligned, the time synchronization error is better than 1 microsecond (Fleming *et al* 2009).

All the data are processed using three different approaches, including the standard RTK estimation (S-RTK), the empirical accelerometer solution (E-ACC) proposed by Wang *et al* (2011), and the enhanced RTK estimation (E-RTK) approaches.
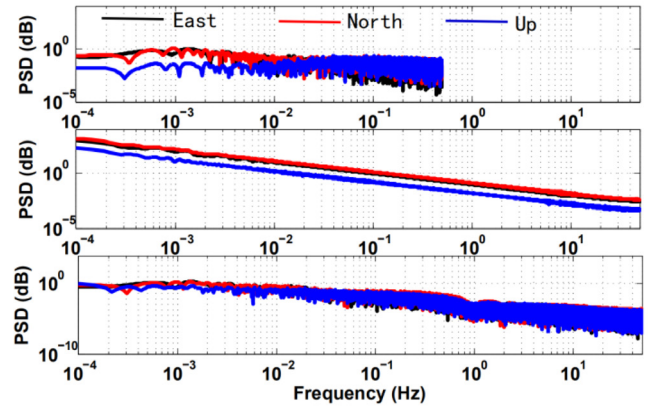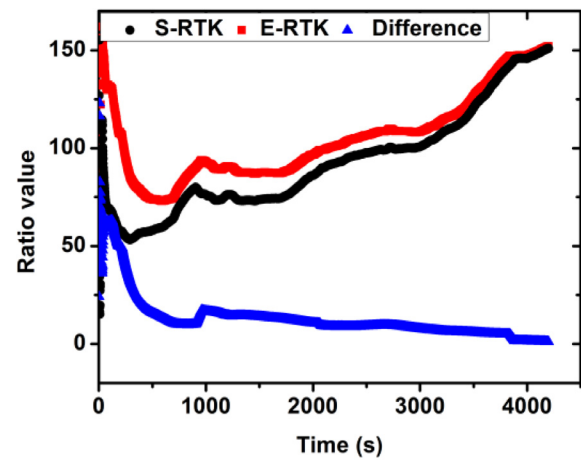
Figure 3. Comparison of the acceleration (top) time series obtained using different approaches and baseline error (bottom) time series in terms of acceleration, velocity and displacement.

3.1. Analysis of the displacement and velocity time series

Figure 2 shows the comparison of the displacement and velocity time series obtained using the different approaches by the whole experiment data. It is clear that the displacement obtained using the E-ACC approach has a large offset (several meters) owing to the baseline error; in addition, the estimated displacements using both the S-RTK and E-RTK approaches have no significant difference. In the bottom of figure 2, we can see the spikes are occurred while there with motions for the E-RTK, but the spikes for the S-RTK are not obvious. In the case of the high-frequency velocity information, the S-RTK approach involves considerable noise; in addition, the details of the motion are not accurately obtained. Further, the E-ACC approach still involves a large offset (several meters per hour for the displacement); however, the acceleration not only with much lower noise, but also with high-resolution (100 Hz), can be helpful to constrain RTK solution, thus the E-RTK approach gets more motion details to show the real velocity variation. The root mean square (RMS) values of the noise for the velocity in the static period are approximately $1.2 \, \text{mm s}^{-1}$, $1.8 \, \text{mm s}^{-1}$, and $2.0 \, \text{mm s}^{-1}$ in the case of the S-RTK approach for the East, North, and Up components,

Figure 4. Comparison of the velocity PSD in the case of different approaches; the graphs are for the S-RTK, E-ACC and E-RTK approaches (top to bottom).
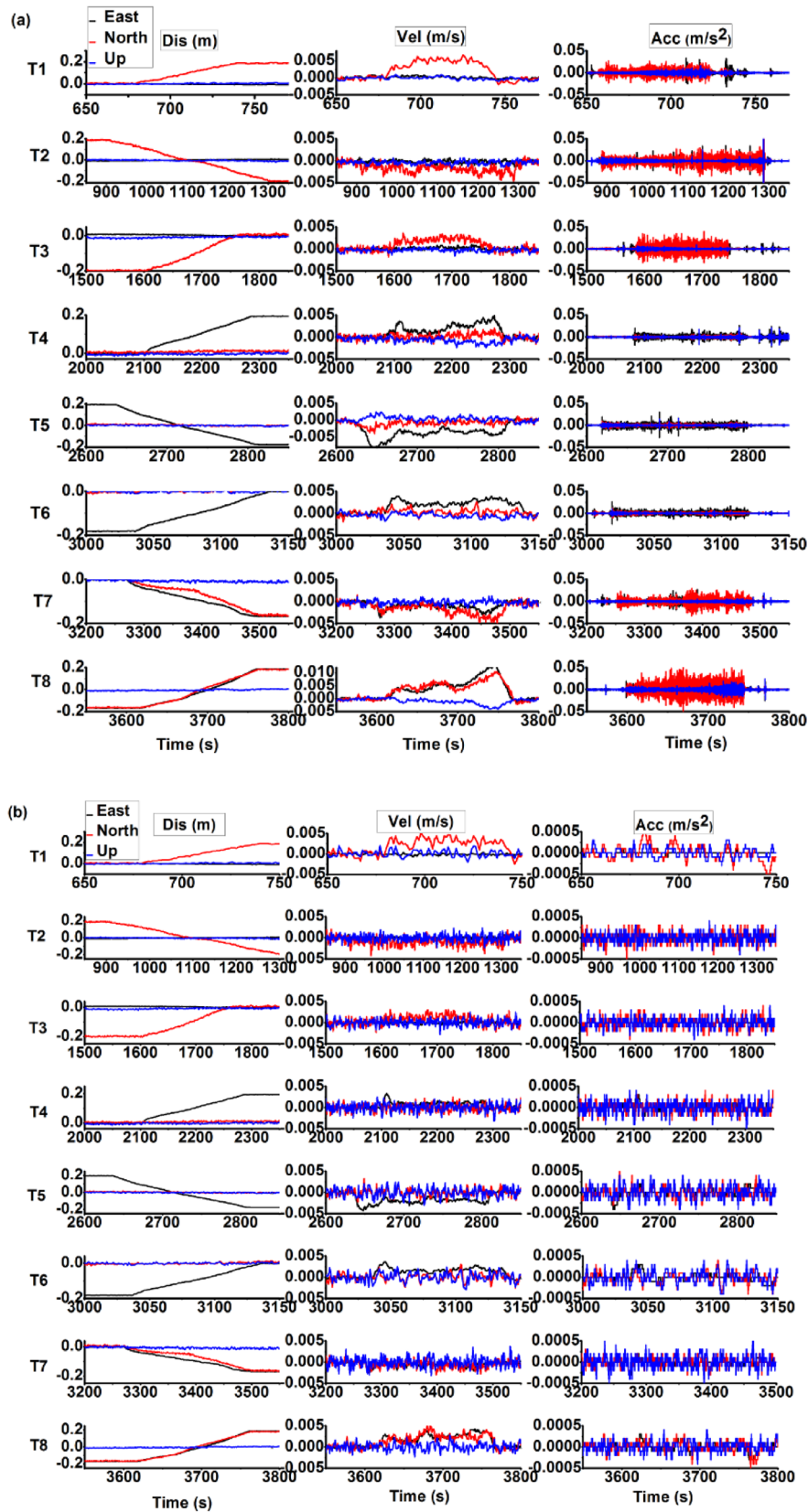

Figure 5. Comparison of ratio values in the case of different approaches.

respectively, whereas, for the E-RTK approach, these are $0.3 \, \text{mm s}^{-1}$, $0.4 \, \text{mm s}^{-1}$, and $0.5 \, \text{mm s}^{-1}$, correspondingly.

3.2. Analysis of the acceleration and baseline error time series

Figure 3 shows the comparison of acceleration and baseline error time series obtained using the different approaches. The spikes in the E-ACC show the largest acceleration observed by the accelerometer which contains the initial baseline error. The spikes in the E-RTK show the largest acceleration estimated by the combination of GNSS and accelerometer observations which not contain the initial baseline error. As expected, in the case of the S-RTK approach, the estimated acceleration includes nearly no signals because of considerable noise, considering that the raw acceleration that is provided by the accelerometer has high resolution, but includes initial baseline errors; in contrast, the obtained acceleration signal using the E-RTK approach is good because it not only reflects the motion status but also does not include baseline errors. The estimated baseline errors in the case of the different approaches are clearly shown in the bottom subfigure

Figure 6. Details of the displacement (left), velocity (middle), and acceleration (right) of the eight simulations depicted graphically; (a) represents the E-RTK approach and (b) represents the S-RTK approach.

Table 1. Quality statistics for the E-RTK and S-RTK approach in the case of all the simulations ('D' indicates displacement (mm), 'V' indicates velocity (mm s^{-1}) and 'A' indicated acceleration (mm s^{-2})).

Test	E-RTK/S-RTK (East)			E-RTK/S-RTK (North)			E-RTK/S-RTK (Up)		
	D	V	A	D	V	A	D	V	A
T1	3.3/3.5	0.3/1.3	0.6/2.4	4.8/5.0	0.4/1.3	0.8/3.0	4.9/5.0	0.5/1.6	0.9/4.0
T2	3.3/3.4	0.3/1.2	0.6/2.4	4.0/4.1	0.4/1.3	0.8/3.3	5.0/5.2	0.5/1.7	0.8/3.6
T3	3.9/4.0	0.3/1.2	0.5/2.1	4.5/4.6	0.4/1.4	0.9/3.5	4.8/5.0	0.5/1.7	0.9/3.8
T4	3.2/3.4	0.3/1.2	0.6/2.3	4.8/4.8	0.4/1.4	0.8/3.2	4.6/4.7	0.5/1.7	0.9/3.7
T5	3.5/3.6	0.4/1.3	0.6/2.5	4.6/4.7	0.5/1.5	0.8/3.3	4.8/4.9	0.6/1.9	0.9/3.8
T6	3.2/3.4	0.4/1.3	0.5/2.3	4.1/4.2	0.5/1.5	0.8/3.4	4.3/4.3	0.5/1.7	0.9/4.0
T7	3.6/3.8	0.4/1.2	0.5/2.5	4.5/4.6	0.5/1.5	0.9/3.6	4.5/4.6	0.5/1.8	0.9/4.1
T8	3.0/3.2	0.4/1.3	0.5/2.5	4.1/4.3	0.5/1.6	0.9/3.8	4.6/4.7	0.5/1.8	0.8/4.0

in figure 3. The bias of the acceleration is approximately several centimeters, whereas the velocity bias is expanded to several decimeters; further, the displacement bias is expanded to several meters. As the baseline bias is changeable due to the tilting, rotation of instrument (Iwan *et al* 1985), it is difficult to precisely model it, thus real-time estimation is the most optimal approach.

3.3. Analysis of the power spectral densities (PSD) of the velocity

Figure 4 shows the power spectral densities of the velocity in the case of the different approaches; in particular, the black, red and blue colors in the figure represent the East, North and Up components, respectively. It can be clearly seen that the E-RTK algorithm adds to the advantages of the other two approaches because it can not only reflect the high-frequency details of the motion but also does so with no system biases.

3.4. Analysis of the ambiguity resolution

Fixing ambiguities is a prerequisite in the case of RTK to achieve high precision positioning results in a short time. In our study, the ratio of the second minimum to the minimum quadratic form of residuals (R-ratio) is used to evaluate the correctness and confidence level of integer ambiguity candidates (Teunissen *et al* 2009). In particular, the ratio value can be considered as an index to denote the reliability of ambiguity resolution; thus, a larger ratio value denotes a more reliable ambiguity resolution. The success rate and the correct-fixing rate of the ambiguity resolution were also assessed, the success ratio threshold is set as 3, and their correctness is based on a discrimination test. As it is a short baseline RTK, and there are also enough BDS satellites, the success rate is 100% and the correct-fixing rate is also 100% for both the S-RTK and E-RTK.

Figure 5 shows the comparison of the ratio values between the S-RTK and E-RTK approaches. The ratio values for the S-RTK approach are shown in black, while the ratio values for the E-RTK approach are shown in red; in addition, their differences are shown in blue. As is clear from figure 5, the ratio values for the S-RTK approach are generally smaller

than those of the E-RTK approach, especially during the start period, where the difference is more than 50; this higher ratio is considered important for fast convergence of the RTK solution. As the estimates converge, their difference becomes smaller, and finally, the ratio values are nearly the same in the case of solutions over a long time.

3.5. Analysis of the displacement, velocity, and acceleration for the all simulations for the proposed approach

Figure 6 shows the displacement, velocity, and acceleration details for all the eight simulations using our proposed E-RTK approach and the traditional S-RTK approach. As expected, the baseline errors of the acceleration values are precisely corrected by the E-RTK; and the high-resolution acceleration measurements are useful in reducing the GNSS noises. Thus, the high-precision and broadband deformation signals (displacement, velocity and acceleration) are recovered in real-time by the E-RTK approach, and for the S-RTK approach, the estimated velocity and acceleration signals with large noises due to the bad signal to noise ratio.

Further, table 1 lists the RMS values for the corresponding estimated values and references. In our study, the static displacement references were provided by the vernier caliper measurements performed on the experiment platform; in addition, the velocity and acceleration references were set as zero when there is no motion. It should be noted that the RMS values are generally less than 5.0 mm for the displacement, better than 0.6 mm s^{-1} for the velocity and smaller than 1.0 mm s^{-2} for the acceleration.

4. Conclusions and discussions

In this study, we proposed an enhanced RTK positioning algorithm by adding high-frequency accelerometer observations; in addition, the baseline error of the acceleration was estimated as an unknown parameter in real-time, which was accounted for in the algorithm. Based on our experiment, we constructed a dataset, which was used for the validation. Based on our analyses, we draw the following conclusions:

(1) Compared with the standard RTK approach, which can only provide high-precision displacement signals, the

proposed E-RTK algorithm can provide high-precision and broadband velocity and acceleration signals as well.

(2) Based on the constraint of high-precision BDS, the baseline error of the accelerometer can be precisely estimated; thus, the high-resolution acceleration can be used to constrain the RTK solution for better ambiguity resolution.

(3) The E-RTK used the broadcast ephemeris, it it easy for real-time operation.

Because the scope of RTK is limited to local areas (<5 km), the E-RTK approach is not suitable for large areas, which is a limitation of our proposed algorithm. As the experiment platform is only an artificial platform, the slide capability in term of frequency is about 1–5 Hz, and the much higher frequency motion (≫1 Hz) should be tested in the future by the automatic platform. Additionally, for the observation noises, dynamic noises are determined by the empirical values in this study; the least-squares variance component estimation can be performed for the robust estimation. In addition, for more robust results, the integration of multi-GNSS and accelerometer data is required.

As the E-RTK can real-time obtain high-precision displacement, velocity and acceleration, it would be interesting to do more works for its application in the future, such as for local area deformation monitoring.

Acknowledgments

ORCID iDs

Rui Tu ⬤ https://orcid.org/0000-0003-4706-5373
Pengfei Zhang ⬤ https://orcid.org/0000-0002-9991-9310

References

Benedetti E, Dermanis A and Crespi M 2017 On the feasibility to integrate low-cost MEMS accelerometers and GNSS receivers *Adv. Space Res.* **11** 2764–78

Bock Y, Melgar D and Crowell B W 2011 Real-time strong-motion broadband displacements from collocated GPS and accelerometers *Bull. Seism. Soc. Am.* **101** 2904–25

Boore D M 2011 Effect of baseline corrections on displacement and response spectra for several recordings of the 1999 Chi–Chi, Taiwan, earthquake *Bull. Seism. Soc. Am.* **91** 1199–211

Chao W, Wu W and Zhao L 2009 An automatic scheme for baseline correction of strong-motion records in coseismic deformation determination *J. Seismo.* **14** 495–504

Elosegui P, Davis J L, Oberlander D, Baena R and Ekstro G 2006 Accuracy of high-rate GPS for seismology *Geophys. Res. Lett.* **33** L11308

Fleming K, Picozzi M, Milkereit C, Kuehnlenz F, Lichtblau B, Fischer J, Zulfikar C, Ozel O and the SAFER and EDIM Working Groups 2009 The self-organising seismic early warning information system (SOSEWIN) *Seismol. Res. Lett.* **80** 755–71

Freybourger M, Hinderer J and Trampert J 1997 Comparative study of superconducting gravimeters and broadband seismometers STS-1/Z in seismic and subseismic frequency bands *Phys. Earth Planet. Inter.* **101** 203–17

Geng J, Bock Y, Melgar D, Crowell B W and Haase S 2013a A new seismogeodetic approach applied to GPS and accelerometer observations of the 2012 Brawley seismic swarm: implications for earthquake early warning *Geochem. Geophys. Geosyst.* **14** 2124–42

Geng J, Melgar D, Bock Y, Pantoli E and Restrepo J 2013b Recovering coseismic point ground tilts from collocated high-rate GPS and accelerometers *Geophys. Res. Lett.* **40** 5095–100

Genrich J F and Bock Y 2006 Instantaneous geodetic positioning with 10–50 Hz GPS measurements: noise characteristics and implications for monitoring networks *J. Geophys. Res.* **111** B03403

Graizer V 2006 Tilts in strong ground motion *Bull. Seism. Soc. Am.* **96** 2090–106

Graizer V M 1979 Determination of the true ground displacement by using strong motion records *Izv Earth Phys.* **25** 26–9

Guo F, Zhang X H, Wang J L and Ren X D 2016 Modeling and assessment of triple-frequency BDS precise point positioning *J. Geod.* **90** 1223–35

Iwan W, Moser M and Peng C 1985 Some observations on strong motion earthquake measurement using a digital accelerograph *Bull. Seismol. Soc. Am.* **75** 1225–46

Larson K M, Bilich A and Axelrad P 2007 Improving the precision of high-rate GPS *J. Geophys. Res.* **112** B05422

Li X, Ge M, Zhang X, Zhang Y, Guo B, Wang R, Klotz J and Wickert J 2013 Real-time high-rate co-seismic displacement from ambiguity-fixed precise point positioning: application to earthquake early warning *Geophys. Res. Lett.* **40** 1–6

Melgar D, Bock Y, Sanchez D and Crowell B W 2013 On robust and reliable automated baseline corrections for strong motion seismology *J. Geophys. Res.* **118** 1177–87

Rizos C 2007 Alternatives to current GPS-RTK services and some implications for CORS infrastructure and operations *GPS Solut.* **11** 151–8

Smyth A and Wu M 2006 Multi-rate Kalman filtering for the data fusion of displacement and acceleration response measurements in dynamic system monitoring *Mech. Syst. Signal Process.* **21** 706–23

Takasu T and Yasuda A 2009 Development of the low-cost RTK-GPS receiver with an open source program package RTKLIB *Int. Symp. on GPS/GNSS (Jeju, South Korea)*

Takasu T and Yasuda A 2010 Kalman filter based integer ambiguity resolution strategy for long-baseline RTK with ionosphere and troposphere estimation *Proc. ION GNSS 2010, Institute of Navigation (Portland, OR, 21–24 September)* pp 161–71

Teunissen P J G and Verhagen S 2009 The GNSS ambiguity ratio-test revisited: a better way of using it *Empire Surv. Rev.* **41** 138–51

Trifunac M D 1971 Zero baseline corrections of strong-motion accelerograms *Bull. Seism. Soc. Am.* **61** 1201–11

Tu R and Chen K 2014b Tightly integrated processing of high-rate GPS and accelerometer observations by real-time estimation of transient baseline shift *J. Navigat.* **67** 869–80

Tu R, Ge M, Wang R and Walter T R 2014a A new algorithm for tight integration of real-time GPS and strong-motion records, demonstrated on simulated, experimental and real seismic data *J. Seismol.* **18** 151–61

Tu R, Liu J, Lu C, Zhang R, Zhang P and Lu X 2017b Cooperating the BDS, GPS, GLONASS and strong-motion observations for real-time deformation monitoring *Geophys. J. Int.* **209** 1408–17

Tu R, Lu C, Zhang P, Liu J and Lu X 2019 The study of BDS RTK algorithm based on zero-combined observations and ionosphere constraints *Adv. Space Res.* **63** 2919–29

Tu R, Wang R, Ge M, Walter T R, Ramatschi M, Milkereit C, Bindi D and Dahm T 2013 Cost-effective monitoring of ground motion related to earthquakes, landslides or volcanic activities by joint use of a single-frequency GPS and a MEMS accelerometer *Geophys. Res. Lett.* **40** 3825–9

Tu R, Zhang P F, Zhang R and Liu J H 2016a The study of key issues about integration of GNSS and strong-motion records for real-time earthquake monitoring *Adv. Space Res.* **58** 304–9

Tu R, Zhang P, Zhang R and Liu J 2016b Comparison of high-rate GPS, strong-motion records and their joint use for earthquake monitoring: a case study of the 2011 Mw 9.0 Tohoku earthquake *Arab. J. Geosci.* **9** 542

Tu R, Zhang R, Lu C, Zhang P, Liu J and Lu X 2017a A unified model for BDS wide area and local area augmentation positioning based on raw observations *Sensors* **17** 507

Uhlemann S, Smith A, Chambers J, Dixon N, Dijkstra T, Haslam E, Meldrum P, Merritt A, Gunn D and Mackay J 2006 Assessment of ground-based monitoring techniques applied to landslide investigations *Geomorphology* **253** 438–51

Wang R, Parolai S, Ge M, Jin M, Walter T and Zschau J 2013 The 2011 Mw 9.0 Tohoku earthquake: comparison of GPS and strongmotion data *Bull. Seismol. Soc. Am.* **103** 1336–47

Wang R, Schurr B, Milkereit C, Shao Z and Jin M 2011 An improved automatic scheme for empirical baseline correction of digital strong-motion records *Bull. Seismol. Soc. Am.* **101** 2029–44

Wellenhof B H, Lichtenegger H and Collins J 2001 *Global Positioning System, Theory and Practice* 5th edn (New York: Springer)

Wilson D, Aster R, Ni J, Schlue J, Grand S, Semken S, Baldridgeand S and Gao W 2002 Broadband seismic background noise at temporary seismic stations observed on a regional scale in the Southwestern United States *Bull. Seismol. Soc. Am.* **92** 3335–42

Wu Y and Wu C 2007 Approximate recovery of coseismic deformation from Taiwan strong-motion records *J. Seismol.* **11** 159–70

Xu P L, Shi C, Fang R X, Liu J N, Niu X J, Zhang Q and Yanagidani T 2013 High-rate precise point positioning (PPP) to measure seismic wave motions: an experimental comparison of GPS PPP with inertial measurement units *J. Geod.* **87** 361–72

Yang Y 2006 *Adaptive Navigation and Kinematic Positioning* (Beijing: The Surveying and Mapping Publishing House)

Zhu L 2003 Recovering permanent displacements from seismic records of the June 9, 1994 Bolivia deep earthquake *Geophys. Res. Lett.* **30** 1740